Coordinated oscillations in cortical actin and Ca2+ correlate with cycles of vesicle secretion

R. Wollman[1,2] and **T. Meyer**[1]

[1]Department of Chemical and Systems Biology, Stanford University, Stanford, CA

Abstract

The actin cortex both facilitates and hinders exocytosis of secretory granules. How cells consolidate these two opposing roles was not well understood. Here we show that antigen activation of mast cells induces oscillations in Ca2+ and PI(4,5)P2 lipids that in turn drive cyclic recruitment of N-WASP and cortical actin oscillations. Experimental and computational analysis argues that vesicle fusion correlates with the observed actin and Ca2+ oscillations. A vesicle secretion cycle starts with the capture of vesicles by actin when cortical F-actin is high, followed by vesicle passage through the cortex when F-actin levels are low, and vesicle fusion with the plasma membrane when Ca2+ levels subsequently increase. Thus, cells employ oscillating levels of Ca2+, PI(4,5)P2 and cortical F-actin to increase secretion efficiency, explaining how the actin cortex can function as a carrier as well as barrier for vesicle secretion.

Regulated exocytosis of secretory granules is a fundamental process of all eukaryotic cells [1]. Successful secretion requires delivery of vesicles from inside the cell to the plasma membrane before fusion can occur. Forty years ago, Orci and collaborators realized that cells have a peripheral microfilament web, later identified as the actin cortex, that acts as a mechanical barrier that prevents dense core secretory vesicles from docking to the plasma membrane (PM) in unstimulated cells [2-8]. This observation contrasted the previously studied synaptic vesicles that were pre-docked at the PM and ready to rapidly fuse. These dense core vesicles are ubiquitously present in cells and are characterized by slower regulated secretion kinetics compared to synaptic vesicles. However, in addition to having a barrier function for vesicles, the actin cortex also acts as a carrier that has to bind myosin V actin motors to capture and transport vesicles to the PM to mediate vesicle fusion [9-15]. This simultaneous function as a barrier for vesicles and as a matrix required for vesicle transport to the PM raises the question of how cells consolidate these opposing barrier and carrier roles of the actin cortex.

[2]Current address, Department of Chemistry and Biochemistry, University of California San Diego, San Diego, CA

Results

Cortical actin acts to facilitate and hinders secretion

We investigated the role of the actin cortex in secretion by focusing on FcεRI-triggered granule exocytosis in rat basophilic leukemia (RBL) cells, a model for studying antigen-triggered mast cell activation and allergic responses[16]. Consistent with a previously proposed barrier role of cortical actin[3-8], depolymerization of cortical actin by addition of Latrunculin caused a small increase in total secretion (Fig. 1a). However, in agreement with a carrier role that increases rather than blocks secretion rates[10-15], the initial rate of exocytosis was reduced after depletion of cortical actin (Fig. 1b-d, Supp Movie 1). Single cell secretion measurements using fluorescent de-quenching of previously endocytosed dextran-FITC showed that activation of the FcεRI receptor results in cell-wide calcium oscillations and exocytosis events that occur at peak calcium in each cycle[17] (Fig. 1e). Based on this pulsatile secretion dynamics, we reasoned that corresponding oscillating changes in the actin cortex may explain why cells have antagonistic barrier and carrier roles of the actin cortex.

Activation of the FcεRI causes oscillation in actin polymerization at the cortex

To investigate the dynamics of the actin cortex during secretion we used live-cell total internal reflection fluorescence (TIRF) microscopy of mCherry-tagged F-Tractin, a biosensor that measures the local concentration of polymerized actin (F-actin)[18-21,22] (Fig. 2a, Supp Fig. 1a-c). In this imaging mode, F-Tractin molecules are selectively excited within ~100 nm of the membrane adhesion surface. Strikingly, antigen stimulation of the FcεRI pathway resulted in regular oscillations (Fig. 2a, right panel, bottom; Supp Movie 2) as well as more irregular pulsatile change in local F-actin concentration (top right panel). Quantitative cluster analysis (see Methods) identified two distinct power spectra patterns (Fig. 2b, left, and Supp Fig. 2). Regular oscillations, mapped to the center region of the adhesion surface while more irregular fluctuations mapped to the peripheral region (Fig. 2b, right). Furthermore, the peripheral F-actin fluctuations operated locally with a characteristic length scale of ~1 μm similar to the spatial range of previously observed lamellipodia dynamics[23,24], whereas the oscillatory region in the center operated globally with a length scale of >5 μm (Fig. 2c; see Methods). The relative change in cortical F-actin concentration during the oscillations was ~15% as estimated from calibration measurements using phalloidin staining (Supp Fig. 1).

Integration of the spatial location of individual vesicle fusion events (Fig. 3a, left and middle panels) showed that exocytosis occurs exclusively in the center and not in the peripheral region (Fig. 3a, right Supp Movie 3). We therefore focused our mechanistic studies on the center region.

Coupled Ca2+, PI(4,5)P2, and N-WASP oscillation drive F-actin dynamics

The observed F-Tractin oscillation time period was reminiscent of the period of antigen triggered Ca2+ oscillations in RBL and other cells[25] (Fig. 1e, Supp Fig. 3 Supp Movie 6). Such Ca2+ oscillations are driven by the generation of Ins(1,4,5)P3 via phospholipase C (PLC)-mediated PI(4,5)P2 hydrolysis, Ins(1,4,5)P3-mediated opening of InsP3-receptor

Ca2+ channels in the endoplasmic reticulum, as well as positive feedback from Ca2+ back to the InsP3 receptor and to phospholipase C. This raised the possibility that Ca2+ oscillation result in oscillations of the levels of PI(4,5)P2 in the plasma membrane. Furthermore, since several regulatory pathways connect PI(4,5)P2 to actin dynamics this raised the possibility that Ca2+ oscillation result in oscillation of plasma membrane concentration of PI(4,5)P2 that then result in oscillatory changes in cortical F-actin. To directly test whether the levels of PI(4,5)P2 oscillate we monitored cortical actin using F-Tractin and PI(4,5)P2 using the biosensor YFP-PH-PLCσ. We found a marked correlation between the two (Fig. 3b, Supp Movie 5) with PI(4,5)P2 increasing first followed by F-Tractin. The average lag between PIP2 and F-Tractin was 11.1±1.5 sec and was statistically significant larger than zero (P-value <0.001, single sample t-test). As a control, we used a second biosensor based on a Tubby domain[26] that binds PI(4,5)P2 with higher selectivity and observed the same oscillations, arguing that the biosensors measure oscillations in PI(4,5)P2 levels (Fig. 3c-e).

Several pathways connect PI(4,5)P2 to actin dynamics. Since the positively charged poly-lysine motif in N-WASP cooperatively binds to plasma membrane PI(4,5)P2[27] in vitro, we tested whether the observed oscillation in PI(4,5)P2 might be responsible for oscillations in recruitment of N-WASP that would then create the observed oscillations in plasma membrane polymerized actin concentration. We imaged the plasma membrane recruitment of fluorescently tagged N-WASP and found that each transient increase in cortical F-actin during the oscillations was preceded by a transient increase in plasma membrane N-WASP concentration (Fig. 4a and Supp Movie 4). The average lag between N-WASP and F-actin was 6.7±1.1 sec (P-value <0.01 for lag bigger than zero). Fig. 4b shows a quantitative analysis of a longer delay from the PI(4,5)P2 increase to the F-Tractin peak compared to the delay from the N-WASP to the F-Tractin peak, consistent with the interpretation that the changes in PI(4,5)P2 drive N-WASP recruitment (P-values <0.05, two sample t-test). Furthermore, partial lowering the levels of PI(4,5)P2 by recruiting the PI(4,5)P2 phosphatase Inp54p to the PM (using a FRB/FKBP dimerization method[23]) reduced the plasma membrane concentration of N-WASP (Fig. 4c). Thus, while additional PI(4,5)P2 sensitive F-actin regulators are likely involved[28], these results suggest that N-WASP is a link between PI(4,5)P2 and F-actin oscillations in the center region of cells.

Together, this data suggest a mechanism for the observed actin oscillations. The positive feedback based Ca2+ oscillation cause oscillations in the plasma membrane concentration of PI(4,5)P2 that then result in oscillatory recruitment of N-WASP to the plasma membrane. N-WASP oscillatory recruitment to the membrane then causes oscillation in cortical actin polymerization. To further test this mechanism we developed an assay that allowed us to visualize this entire pathway live in a single cell by performing a simultaneous 5-channel live-cell monitoring of cytoplasmic Ca2+ levels using Fura-2 by epi-fluorescence imaging and N-WASP, F-Tractin, and PH-PLCδ by TIRF imaging. As predicted by this model, all four signals oscillated with the same frequency but shifted phases (Fig. 5,6). Pharmacological agents were then used to further test this model by inhibiting the oscillations at different levels in the pathway. Inhibition of N-WASP dynamics using the small molecule inhibitor Wiskostatin, Fig. 5a) dissociated N-WASP from the plasma membrane, blocked F-actin oscillations and reduced total cortical F-actin without affecting

Ca2+ or PI(4,5)P2. Similarly, rapamycin-mediated PM recruitment of an inhibitory N-WASP-FKBP12 fusion construct[29] suppressed actin oscillations without affecting Ca2+ or PI(4,5)P2 oscillations (Fig. 5b). Addition of the ER Ca2+ pump inhibitor Thapsigargin rapidly stopped all four oscillations (Fig. 6a). This argued that the observed PI(4,5)P2 oscillations are likely a result of Ca2+ oscillations periodically activating Ca2+-sensitive PLC. Finally blocking the most downstream oscillation of F-actin by addition of or of Latrunculin-B (Fig. 6b) or Cytochalasin D (Fig. 6c), showed that oscillations in Ca2+, PI(4,5)P2, and N-WASP continued after inhibition of actin oscillations as predicted by the linear pathway mechanism. Thus, linked Ca2+ and PI(4,5)P2 oscillations function as drivers of cortical F-actin oscillations in the center adhesion surface (Fig. 6d).

To map the sequence of events during each of the oscillation cycles, we averaged the signals from different cycles using the peak Ca2+ level as an anchor (Fig. 6e). This analysis showed that a Ca2+ increase (orange) and concomitant PI(4,5)P2 reduction (cyan) precede the drop in PM localized N-WASP (purple), which in turn precedes a drop in F-actin polymerization (green). As Ca2+ level decrease and PI(4,5)P2 levels increase, N-WASP is again recruited to the PM, followed by an increase in F-actin polymerization.

Computational model linking oscillating cortical actin to enhanced secretion efficiency

We next hypothesized that coupled Ca2+ and actin oscillations may explain the antagonistic barrier and carrier function of the actin cortex. We reasoned that oscillatory actin dynamics would allow cytoplasmic vesicles to be captured when actin is elevated, pass to the PM when cortical actin is lowered and fuse with the PM when Ca2+ is subsequently increased. To evaluate how such a system may work, we constructed a simplified mathematical model (Fig. 7a-b; Supp Note). The scheme in Fig. 7a shows how the model defines F-actin and Ca2+ dependencies of the vesicle capture, passage and fusion rates (Fig. 7a). The model uses the experimentally measured (Fig. 6d) phase-shifted F-actin and Ca2+ oscillations as inputs (Fig. 7b, top) and describes the transition to the actin cortex bound state, Vcortex (Fig. 7b, middle), to the docked state at the plasma membrane, V_{pm} (Fig. 7b, middle) and, as functional output, the fusion of the docked vesicles (Fig 7b, bottom). The simulations in Fig. 7b show how F-actin and Ca2+ oscillations can create a three-stroke cycle of capture, passage, and fusion of secretory vesicles. During each cycle, vesicles are captured as the level of F-actin increases, a fraction passes through the cortex as cortical actin levels decrease, and then fuses as the phase-shifted Ca2+ signal increases. This sequential mechanism provides an explanation of how oscillations, compared to constant levels of F-actin and calcium, can enhance the average secretion rate (Fig. 7c, Supp Fig. 4).

We tested the model assumption that vesicle capture is cyclic by monitoring GFP-Myosin Va, a previously described motor protein that binds vesicles to the actin cortex and also locally transports vesicles[9]. Knockdown of Myosin Va expression caused a small but significant reduction in secretion (Supp Fig 4a). This effect was similar in magnitude to the reduction seen when N-WASP was knocked down or inhibited using Wiskostatin (Supp Fig 4b). Furthermore, most of the antigen-triggered recruitment of myosin Va to the cortex occurred in the center of the adhesion region (Fig. 7d, left, Supp Fig 4c), overlapping with the region where most of the vesicle fusion occurs (Fig. 3a). Finally, a statistical analysis

showed that myosin Va recruitment occurs preferentially during peak compared to trough F-actin levels during oscillations (Fig. 8d, right) supporting the model assumption of a cyclic capture of vesicles at peak levels of F-actin.

We then tested the prediction that oscillations make secretion more effective by comparing secretion rates in cells with oscillating Ca2+ levels to cells with persistently elevated Ca2+ levels. Both types of cells can be found in response to the same antigen stimulus. Indeed, oscillating cells (blue, Fig. 8a, Supp Fig 5) show ~30% higher secretory rates compared to cells with persistently elevated Ca2+ levels (red). To directly compare secretion during oscillatory Ca2+/F-actin changes versus persistent Ca2+ elevation, we added the ER Ca2+ pump blocker Thapsigargin which increases Ca2+ levels and found that cells with oscillations prior to the addition of Thapsigargin subsequently reduced exocytosis rates to levels comparable to non-oscillating cells (Supp Movie 7). An example trace is shown in Fig. 8b where addition of Thapsigargin keeps Ca2+ at a persistently high level while reducing the rate of secretion (Fig. 8c). We further tested whether the advantage of oscillating cells is eliminated when we block actin oscillations with either an actin polymerization inhibitor Cytochalasin D, or an actin filament stabilizer Jasplakinolide (Fig. 8b). Both inhibitors reduced the secretion rates of oscillating cells by approximately ~30% to the same rate as those of non-oscillating cells (Fig. 4a). In agreement with a barrier role of the actin cortex, Jasplakinolide, which stabilizes cortical actin, reduced secretion in both cases even further (Fig. 8a,c).

Discussion

The evolution of biological control systems such as the one of regulated secretion involves optimization between conflicting requirements. Our study suggests that an oscillating systems design can be employed by cells to optimize the reliability and efficiency of dense core vesicle secretion. The challenge for regulated secretion is that the actin cortex is critically required for cells to maintain cell shape and prevent the formation of membrane blebs [30]. Yet, as appreciated 40 years ago by Orci et al [2], the same cortical actin that is critical for a cells integrity prevents the access of secretory granule to the plasma membrane. This barrier effect of the actin cortex is likely important in many cell types to minimize inadvertent secretion in response to short stimuli that are too short or weak to lower the barrier. At the same time, secretory granules need to be transported from the cell interior to the vicinity of the plasma membrane in a process requiring microtubules to get the vesicles closer to the periphery and actin motor-mediated transport to get them docked to the plasma membrane [1]. This apparent barrier-carrier paradox provides therefore an excellent example for the evolution of dynamic regulatory strategies to optimize cell function given multiple constraints on the system.

Our study introduces a dynamic secretory systems design that uses oscillations in cortical actin to temporally partition the opposing functions of the actin cortex. We show that cells employ phase-shifted oscillations of Ca2+, PI(4,5)P2, N-WASP, and F-actin to enhance secretion. The coupled Ca2+ and F-actin oscillations correlate with a vesicle secretion recruitment and fusion engine that repeatedly transitions between three strokes: capture at high F-actin, passage through the actin cortex at low F-actin levels, followed by Ca2+-

triggered fusion (Fig. 8D). Thus, cells can consolidate opposing roles of a control element by oscillating its concentration and temporally partition the associated regulatory processes. Given the ubiquitous presence of oscillating systems in biology, it can readily be envisioned that many of them evolved to resolve similar opposing constraints. As in the case of dense core vesicle secretion, such optimized oscillatory systems have likely a general role in enhancing the effectiveness and robustness of different cellular outputs.

Methods

Nucleic acid reagents

mTurquoise-NWASP, mCitrine-NWASP, mCitrine-PHplcδ, and mTurquoise-PHplcδ were cloned into Clontech-C1-like mTurquoise and mCitrine vectors. F-Tractin-GFP was the kind gift of Michael Shell and was sub-cloned to replace the fluorescent protein with mCerulean, mCherry, and tdTomato. GFP-Myosin Va was kind gift of James Spudich. siRNA reagents for N-WASP were purchased from Sigma Aldrich (cat # SASI_Rn02_00251193, GGAACAAGAGCTATACAAT and SASI_Rn02_00251194, GGGAACAAGAGCTATACAA). siRNA against MyosinVa were purchased from Dharmacon (cat # MQ-094195-00-0005, GAUUAGAGGUGCUGAACUG, GAUCAGCGCAGCAGGGUUU, CCAAACUCAUUUAUACGUA, GCACAAGCAUAUAUUGGUU). Control non-targeting siRNA was purchased from Dharmacon (cat# D-001206-14-05, UGGUUUACAUGUCGACUAA).

Chemicals

Fura-2, Flou-4 calcium dyes were used at 1-4 μM and Thapsigargin was used at 1μM. (Invitrogen). The N-WASP inhibitor Wiskostatin (Sigma) was used at 8.33 μM. Latrunculin B (used at 4 μM), Cytochalasin D (used at 2.5 μM), and Jasplakinolide (used at 2 μM) were purchased from EMD Chemicals.

Cell culture & electroporation

RBL-2H3 cells (ATCC) were cultured in DMEM supplemented with 10% FBS (Invitrogen). In all experiment with the exception of Fig. 1, cells were sensitized overnight with anti-TNP IgE (BD Biosciences) and stimulated by the addition of 10-100 ng/ml multivalent BSA-TNP with loading of 26 TNPs per BSA (Biosearch Technologies). Pharmacological activation in Fig 1 was done with 1 μM Ionomycin and 100 ng/ml PdbU (Sigma). For all fluorescent reporter experiments and siRNA knockdowns, cells were electroporated using Amaxa nucleufactor following manufacturer instructions (kit T, program X001).

Microscopy

Cells were imaged using a custom-built prism TIRF microscope with 5 laser lines (442, 473, 514, 532, and 650). The microscope was equipped with a Lambda Sutter LS arclamp with an internal filter wheel and an additional emission filter wheel controlled using a Lambda Sutter 10-2. Images were captured using a QuantEM EM-CCD camera from photometrics. A schematic of the light path is shown in Supp Fig 6. Estimation of channel bleed-through on this microscope is provided in Supp Fig. 7. Lasers were combined on an optical table using Semrock LaserMUX single edge dichroic mirrors. Each laser was controlled by a

Vincent shutter controlled using a D122 or D1 control boxes. As the communication speed with the D122 is relatively slow (max baud rate of 300 char/sec) all laser shutters were controlled using TTL signal generated using an Arduino control board. To combine epi-fluorescent we added a 10/90 broad spectrum beamspliter configured such that 10% of epi excitation light passed to the sample and 90% of emission light passed to the camera. Emission filters are shown in Supp Fig 6b. Exposure times were 100-500 milliseconds using gain values of 250-500. The duration between two consecutive frames was less than 5 seconds. A histogram of actual frame difference time for a representative experiment is shown in Supp Fig 6c.

The microscope was controlled using a custom Matlab interface to the open-source Micro-manager software[21]. During acquisition, immediately after each frame was transferred from the camera to the computer RAM, a timestamp was recorded. Imaging was done using water dipping 60x and 10x objective for the high and low resolution imaging respectively. Cells were labeled with WGA-647 (Invitrogen) that was used with a 650nm laser line for image-based autofocus. During time-lapse acquisition an image based autofocus correction was employed by performing an 8 micron Z-sweep to identify the Z-point of maximal contrast. Autofocus was performed every ~30-60 seconds automatically during acquisition only in high resolution (60x) imaging.

Secretion assays

Total secretion experiments were performed using an enzymatic assay to measure total secretion of β-hexoamidase. Secretion was measured using 2.5 μM of 4-Methylumbelliferyl N-acetyl-β-D-glucosaminide (MUG, Sigma), a compound that changes it fluorescent properties after it is processed by secreted enzyme β-hexoamidase. Fluorescence was measured using a Victor3 plate reader from PerkinElmer. In each well the secretion level after stimulus was normalized to total β-hexoamidase after cell permeabilization using 1% Triton Secretion rate experiments were done by measuring the disappearance rate of secretory granule marker, LysoTracker-Red (Invitrogen) using low resolution (10x) TIRF microscopy. LysoTracker marks all low-pH organelles in the cells, when imaged in TIRF, due to the thin optical section, LysoTracker predominantly marks secretory granules. Time-lapse stacks were segmented to identify single cells and the total loss of initial SG intensity was quantified over time.

Exocytosis assays

Dextran-FITC (Sigma) exocytosis assays were done after incubating cells with 1 mg/ml dextran-FITC for 48 hours using a protocol kindly provided by David Holowka, Cornell University. Time lapse stacks were segmented to identify single cells and the intensity of dextran-FITC was measured using continuous TIRF imagining of the green channel that were interrupted every 3-5 seconds to acquire the Fura-340 and Fura-380 epi fluorescence channels. Exocytosis was quantified by first identifying peaks in each cells' dextran-FITC intensity time series. Peaks were defined as local maxima above a threshold to eliminate noise. To correct for differences in the loading of dextran-FITC between experiments, the number of peaks in each cells was divided by the average number of peaks per cell in a

movie. Oscillatory cells were identified based on the Fura-2 ratio time-series using a spectrogram analysis with a frequency window of 1/15 to 1/60 seconds.

Image analysis and initial data processing

All images were corrected for uneven illumination and photobleaching as a first step before any further analysis was performed. Uneven illumination was corrected using a background subtraction procedure. To estimate the background, a non-parametric model for the uneven illumination that is based on thin-plate 2d splines was estimated and subtracted from all frames. Photo-bleaching correction of TIRF stacks was corrected using epi-fluorescent images of the same channel. Epi images were collected once every thirty TIRF images. Interpolation of the loss of fluorescence in the epi images was used to correct the TIRF stacks. Additional analysis was performed on each cell separately. Cell masks were estimated for each frame using a combination of user specified boundaries and segmentation of one of the channels using a Gaussian mixture model (GMM) segmentation algorithm. GMM segmentation was able to accurately separate a cell from the background but is unable to separate touching cells. Touching cells were separated using a polygon ROI. The final cell mask was defined as all the foreground pixels identified by the GMM algorithm that are within the user specified polygon. In cases were x-y drift was a concern, images were registered using a sequential normalized cross-correlation algorithm. All analysis was done using custom Matlab programs using the image analysis and signal processing toolboxes.

Time series processing

Time series data was estimated either per pixel or for a user defined region or interest. The pixel intensity data per frame and the timestamp for that frame were used to "gridify" the data. An equal spacing time grid was chosen (Tgrid) such that the dt in the grid is the average time difference between channels. Then a linear interpolation procedure was employed for each channel time series separately to estimate the channel intensities on the time grid Tgrid. This procedure resulted in a matrix where all intensities are from the same time point. This interpolated matrix was then used for further analysis. This analysis procedure made the analysis independent of the order of channel acquisition. Example of a timeseries acquisition times and the gridified matrix is shown in Supp Fig. 14d. For the cross-correlation analysis, high-pass filter was applied to the time-series and the output was normalized to a maximal autocorrelation value of 1. To aid visualization of the oscillatory dynamics all time-series data were filtered using a high-pass filter with a width >300 seconds. Example of analysis routine with intermediate results is provided in Supp Fig 8.

Cluster analysis of fluctuation actin regions

Time-lapse images were first corrected for uneven illumination and photo-bleaching and registered in x-y as described above. The aligned stack was used to create ~12,000 time series for intensity changes for the biosensor F-Tractin. Frequency power spectrum analysis was used to identify the regularity of the oscillation and their major period. In addition, the range (1%-99% percentile interval) was calculated for all the time series. These three dimensions (regularity, major period and range) were used as inputs to a Gaussian mixture model clustering for 2 populations. The boundary between the two populations was the two

dimensional manifold were posterior distribution for each of the two populations was 0.5. Supp Fig 3 shows an example of a scatter plot used for clustering.

Spatial correlation analysis

Correlation coefficient between every two time-series in the cells as well as their Euclidean distance was measured (~80,000,000 pairs per cell). The data was binned (single pixel-size width; 0.26 μm) and fitted with an exponentially decaying function (Fig 2c). The length scale was defined as the distance over which the correlation decays.

Measurement of F-actin levels after Thapsigagin and EGTA treatment

Cells were sensitized with IgE overnight and stimulated with TNP-BSA similar to live cell analysis. 10 min after TNP stimulation, Thapsigargin (1 μM) with and without 10 mM EGTA or buffer control were added to cells. 5 minutes after drug addition cells were fixed and stained with DAPI and phalloidin alexa-594 according to manufacturer protocol. Several hundred cells (743 for control, 895 for Thaps+EGTA and 1559 for Thaps) were imaged per treatment. Binary masks were generated using otsu thresholding on the DAPI intensity and the phalloidin intensity within each mask per cell was quantified.

Statistical analysis

The following statistical tests where used throughout the paper:

To test for existence of a lag, cross correlation analysis on two time series was performed (as explained above) for multiple cells. In each cell, the cross-correlation analysis provided a single value of lag where cross-correlation is maximal. Using this population of lags, a single sample t-test was used to estimate if the lag value is significantly different than zero. This test was performed in Fig. 2b, 2c. P-values shown in Fig. 2d are the values that the lags between N-WASP and F-actin and between PIP2 and N-WASP were significantly different from zero.

To test the difference between lags of different biosensors, first a population of lags for each marker was estimated as described above and a statistical test to compare the two populations was performed. In Fig. 2d we show average lag values and therefore use parametric two sample t-test. In Supp Fig. 5c due to existence of a few outliers, the median value is presented and non-parametric Wilcoxin rank-sum test was performed.

To test the significance of different treatment on β-hexoamidase secretion (supp fig 1 & 10) multiple wells were measured and a two-sample t-test was performed comparing each of the treatment against controls.

To test the significance of the change in cortical F-actin after treatment with Thapsigargin (Supp Fig. 4a) and Thapsigargin + EGTA cell were treated as described above and two sample t-tests were performed comparing them to control cells.

Supplementary Material

Refer to Web version on PubMed Central for supplementary material.

References

1. Morgan A, Burgoyne RD. Secretory Granule Exocytosis. Physiological Reviews. 2003; 82:581–632. [PubMed: 12663867]

2. Orci L, Gabbay KH, Malaisse WJ. Pancreatic beta-cell web: its possible role in insulin secretion. Science (New York, N.Y.). 1972; 175:1128–1130.

3. Cheek TR, Burgoyne RD. Nicotine-evoked disassembly of cortical actin filaments in adrenal chromaffin cells. FEBS letters. 1986; 207:110–114. [PubMed: 3770186]

4. Koffer A, Tatham PE, Gomperts BD. Changes in the state of actin during the exocytotic reaction of permeabilized rat mast cells. The Journal of cell biology. 1990; 111:919–927. [PubMed: 2391368]

5. Chowdhury HH, Popoff MR, Zorec R. Actin cytoskeleton depolymerization with clostridium spiroforme toxin enhances the secretory activity of rat melanotrophs. The Journal of physiology. 1999; 521(Pt 2):389–395. [PubMed: 10581310]

6. Frigeri L, Apgar JR. The role of actin microfilaments in the down-regulation of the degranulation response in RBL-2H3 mast cells. Journal of immunology (Baltimore, Md. :. 1999; 162:2243–2250. 1950.

7. Becker KA, Hart NH. Reorganization of filamentous actin and myosin-II in zebrafish eggs correlates temporally and spatially with cortical granule exocytosis. Journal of cell science. 1999; 112(Pt 1):97–110. [PubMed: 9841907]

8. Nishida K, et al. Fc{epsilon}RI-mediated mast cell degranulation requires calcium-independent microtubule-dependent translocation of granules to the plasma membrane. The Journal of cell biology. 2005; 170:115–126. doi:10.1083/jcb.200501111. [PubMed: 15998803]

9. Eichler TW, Kögel T, Bukoreshtliev NV, Gerdes H-H. The role of myosin Va in secretory granule trafficking and exocytosis. Biochemical Society transactions. 2006; 34:671–674. doi:10.1042/BST0340671. [PubMed: 17052171]

10. Narasimhan V, Holowka D, Baird B. Microfilaments regulate the rate of exocytosis in rat basophilic leukemia cells. Biochemical and biophysical research communications. 1990; 171:222–229. [PubMed: 2203345]

11. Li G, et al. Effect of disruption of actin filaments by Clostridium botulinum C2 toxin on insulin secretion in HIT-T15 cells and pancreatic islets. Molecular biology of the cell. 1994; 5:1199–1213. [PubMed: 7865885]

12. Oheim M, Stühmer W. Tracking chromaffin granules on their way through the actin cortex. European biophysics journal : EBJ. 2000; 29:67–89. [PubMed: 10877017]

13. Lang T, et al. Role of actin cortex in the subplasmalemmal transport of secretory granules in PC-12 cells. Biophysical journal. 2000; 78:2863–2877. doi:10.1016/S0006-3495(00)76828-7. [PubMed: 10827968]

14. Nightingale TD, et al. Actomyosin II contractility expels von Willebrand factor from Weibel-Palade bodies during exocytosis. The Journal of Cell Biology. 2011; 194:613–629. doi:10.1083/jcb.201011119. [PubMed: 21844207]

15. Masedunskas A, et al. Role for the actomyosin complex in regulated exocytosis revealed by intravital microscopy. Proceedings of the National Academy of Sciences of the United States of America. 2011; 108:13552–13557. doi:10.1073/pnas.1016778108. [PubMed: 21808006]

16. Rivera J, Fierro NA, Olivera A, Suzuki R. New insights on mast cell activation via the high affinity receptor for IgE. Advances in immunology. 2008; 98:85–120. doi:10.1016/S0065-2776(08)00403-3. [PubMed: 18772004]

17. Kim TD, Eddlestone GT, Mahmoud SF, Kuchtey J, Fewtrell C. Correlating Ca2+ responses and secretion in individual RBL-2H3 mucosal mast cells. J Biol Chem. 1997; 272:31225–31229. [PubMed: 9395446]

18. Johnson HW, Schell MJ. Neuronal IP3 3-kinase is an F-actin-bundling protein: role in dendritic targeting and regulation of spine morphology. Mol Biol Cell. 2009; 20:5166–5180. doi:E09-01-0083 [pii] 10.1091/mbc.E09-01-0083. [PubMed: 19846664]

19. Rak GD, Mace EM, Banerjee PP, Svitkina T, Orange JS. Natural killer cell lytic granule secretion occurs through a pervasive actin network at the immune synapse. PLoS Biol. 2011; 9:e1001151. doi:10.1371/journal.pbio.1001151 PBIOLOGY-D-11-00213 [pii]. [PubMed: 21931536]

20. Lazarides E, Weber K. Actin antibody: the specific visualization of actin filaments in non-muscle cells. Proc Natl Acad Sci U S A. 1974; 71:2268–2272. [PubMed: 4210210]

21. Edelstein A, Amodaj N, Hoover K, Vale R, Stuurman N. Computer control of microscopes using microManager. Curr Protoc Mol Biol. 2010 **Chapter 14**, Unit14 20, doi: 10.1002/0471142727.mb1420s92.

22. Snapper SB, Rosen FS. The Wiskott-Aldrich syndrome protein (WASP): roles in signaling and cytoskeletal organization. Annu Rev Immunol. 1999; 17:905–929. doi:10.1146/annurev.immunol. 17.1.905. [PubMed: 10358777]

23. Ponti A, Machacek M, Gupton SL, Waterman-Storer CM, Danuser G. Two distinct actin networks drive the protrusion of migrating cells. Science. 2004; 305:1782–1786. doi:10.1126/science. 1100533 305/5691/1782 [pii]. [PubMed: 15375270]

24. Giannone G, et al. Periodic lamellipodial contractions correlate with rearward actin waves. Cell. 2004; 116:431–443. doi:S0092867404000583 [pii]. [PubMed: 15016377]

25. Meyer T, Stryer L. Calcium spiking. Annu Rev Biophys Biophys Chem. 1991; 20:153–174. doi: 10.1146/annurev.bb.20.060191.001101. [PubMed: 1867714]

26. Chapman ER. Synaptotagmin: a Ca(2+) sensor that triggers exocytosis? Nat Rev Mol Cell Biol. 2002; 3:498–508. doi:10.1038/nrm855 nrm855 [pii]. [PubMed: 12094216]

27. Papayannopoulos V, et al. A polybasic motif allows N-WASP to act as a sensor of PIP(2) density. Mol Cell. 2005; 17:181–191. doi:S1097276504007993 [pii] 10.1016/j.molcel.2004.11.054. [PubMed: 15664188]

28. Janmey PA, Lindberg U. Cytoskeletal regulation: rich in lipids. Nat Rev Mol Cell Biol. 2004; 5:658–666. doi:10.1038/nrm1434. [PubMed: 15366709]

29. Suh BC, Inoue T, Meyer T, Hille B. Rapid chemically induced changes of PtdIns(4,5)P2 gate KCNQ ion channels. Science. 2006; 314:1454–1457. doi:10.1126/science.1131163. [PubMed: 16990515]

30. Sheetz MP, Sable JE, Dobereiner HG. Continuous membrane-cytoskeleton adhesion requires continuous accommodation to lipid and cytoskeleton dynamics. Annual review of biophysics and biomolecular structure. 2006; 35:417–434. doi:10.1146/annurev.biophys.35.040405.102017.

Author Manuscript

Author Manuscript

Author Manuscript

Author Manuscript
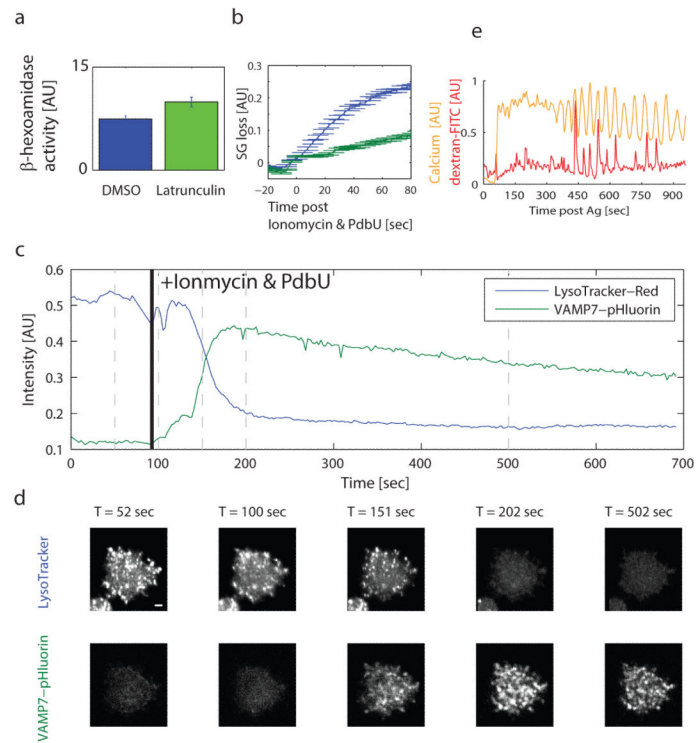
Figure 1. Depolymerization of cortical F-actin increases total amount of secreted enzyme but with slower initial kinetics

a Population measurement of total secreted β-hexoamidase 30-min past pharmacological activation with Ionomycin (1μM) and PdbU (100ng/ml) addition to cells pre-treated with 4 μM Latrunculin (green) or DMSO control (blue). (P-value <0.001, two sample t-test, error-bars s.e.m, N=64). **b** Time courses of initial loss of secretory granule monitored with LysoTracker. Loss of SG is defined as the relative drop in fluorescent intensity from the intensity prior to antigen addition. Cells were stimulated with Ionomycin (1μM) and PdbU (100 ng/ml); control (DMSO) and Latrunculin A (4 μM) pre-treated (5 min prior to drug addition) cells shown in blue and green, respectively. Errorbars show the 95% confident intervals (N=1258 & 2623). **c-d** Disappearance of secretory granule marker LysoTracker corresponds to an increase in exocytosis marker VAMP7-pHlourin. **c** Time series of secretory granule marker (SG) and pH sensitive VAMP7-pHlourin. Black vertical line marks the addition of 1μM Ionomycin and 100 ng/ml PdBU. Dashed lines show time-points of snapshots shown in **d** Scale-bar 5 μm. Note that both panel **a** and **c** are based on LysoTracker marking of SG, with panel **a** shows the loss of SG and panel **c** shows remaining SG intensity to correspond to the images in **d**. **e** Time series of Calcium (orange) signals and dextran-FITC (red) release following activation of the mast cell receptor FcεRI. The increase in pH during vesicle fusion results in de-quenching of FITC, causing a transient fluorescent secretion signal.
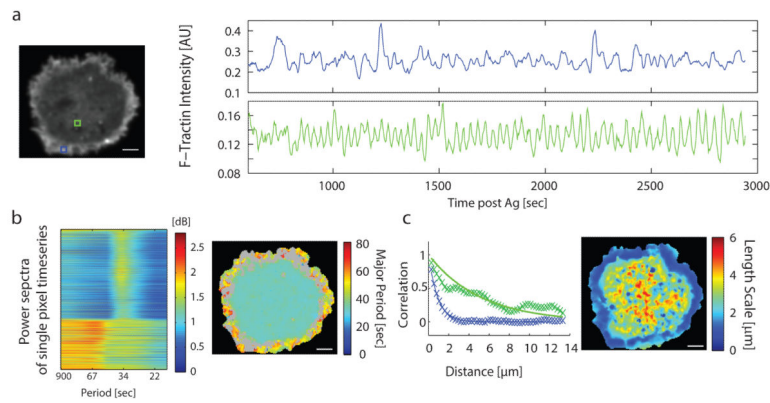
**Figure 2. Receptor-stimulated cell-wide and local F-actin oscillations**
a Live measurements of local cortical F-actin oscillations using F-Tractin biosensor and TIRF optical sectioning (left). Distinct local cortical F-actin concentration changes are observed at different sites, two representative regions of interests are shown in blue in the periphery and green in the cell center (right). **b** Two types of F-actin oscillations with distinct power spectra. Amplitudes of the power spectra (decibel, dB) were converted to a color code (left panel, x-axis; period time labels) for each pixel in a cell (y-axis), and clustered into 2 groups. The two subtypes of oscillations map to center and peripheral cell adhesion regions, respectively. Map (right) shows the projection of the major period of each local F-Tractin power spectra onto the cell image. **c** Oscillations are synchronized between pixels across the entire center region but not in the peripheral region. Panel on left shows single site examples with exponential fits to the spatial correlation function for pixels in the center and peripheral regions, respectively. Image on right shows a map of the fitted spatial correlation length for each pixel. Scale-bar 5 μm.
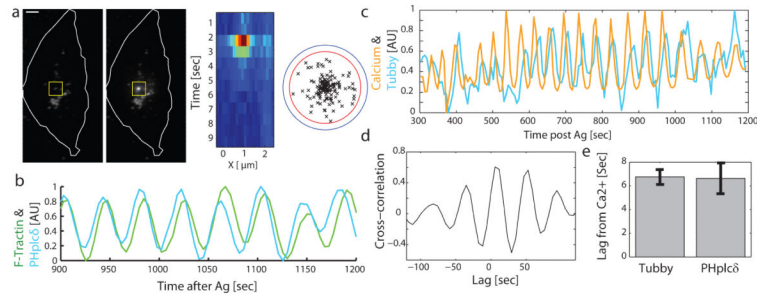
Figure 3. Oscillations in PI(4,5)P2 lipid precede F-actin oscillations

a Secretion occurs exclusively in the center and not peripheral region. Left two panels show a cell loaded with the secretory marker dextran-FITC before (left) and 1 second (middle) after an exocytosis event, scale-bar 5 μm, exocytosis event is marked by a yellow box. Kymograph in middle is taken through the center of the yellow box. The right shows a map projecting 155 exocytosis events from 12 cells according to their distance from the periphery (monitored in the first 20 minutes after antigen addition). The red line marks the normalized area where central F-actin oscillations are observed. **b** Synchronized phase-shifted oscillations in PI(4,5)P2 (monitored with PH-PLCδ) and cortical F-actin. **c** Example of a time series of signals measured with Epi-fluorescent of Fura-2 (orange; Ca2+ signals) and a second PI(4,5)P2 biosensor, the Tubby domain from the Tubby protein tagged with YFP and imaged in TIRF (cyan). Raw data for panels b & c is presented in Supp Table 1 **d** Cross-correlation between the time series shown in **c** was used to estimate the lag and significance of the correlation between the two time series. **e** Comparison of the lag between calcium and PH-plcδ to that between calcium and Tubby domain. Bars show median lag and errorbars are the median absolute deviation. P-value = 0.57, Wilcoxon rank sum test, N=15.
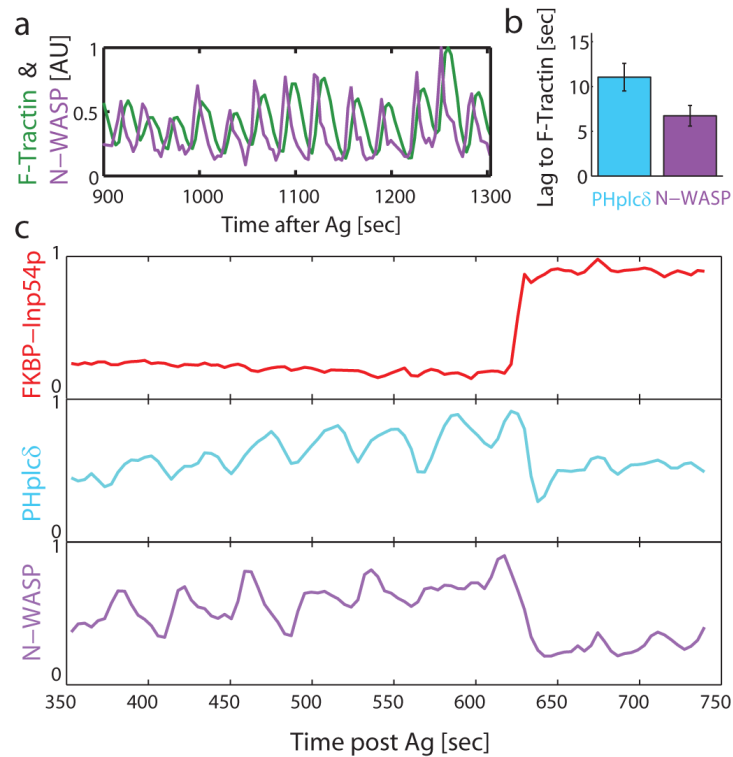
Figure 4. Oscillation in PM levels of N-WASP connect PI(4,5)P2 and F-actin oscillations
a Synchronized phase-shifted oscillations in N-WASP (purple) and cortical F-actin (F-Tractin, green) concentration in center region **b.** PI(4,5)P2 signals are followed by N-WASP recruitment and then F-actin polymerization. Lags between N-WASP and PHplcd to F-Tractin were significantly bigger than zeros (P-values <0.05 N=8 and P-value < 0.01 N=7 respectively) with the average lag between PHplcd and F-Tractin significantly bigger than the lag between N-WASP and F-Tractin (P-value <0.05, N=15, errorbars show s.e.m.). **c** A reduction in PI(4,5)P2 by forced translocation of a 5′PIP2 phosphatase rapidly decreases N-WASP PM localization. Partial recruitment of YFP-FKBP-Inp54p to the plasma membrane (upper panel) by the addition of 0.5 μM rapamycin (to trigger binding to PM localized FRB) (T=620) triggers a small reduction in the levels of PI(4,5)P2 as reported by the PH-plcδ-mTurquoise biosensor (middle panel). A small relative reduction in PI(4,5)P2 was sufficient to cause a rapid reduction in the localization of mCherry-N-WASP to the plasma membrane (lower panel). Raw data for panels a & c is presented in Supp Table 1.
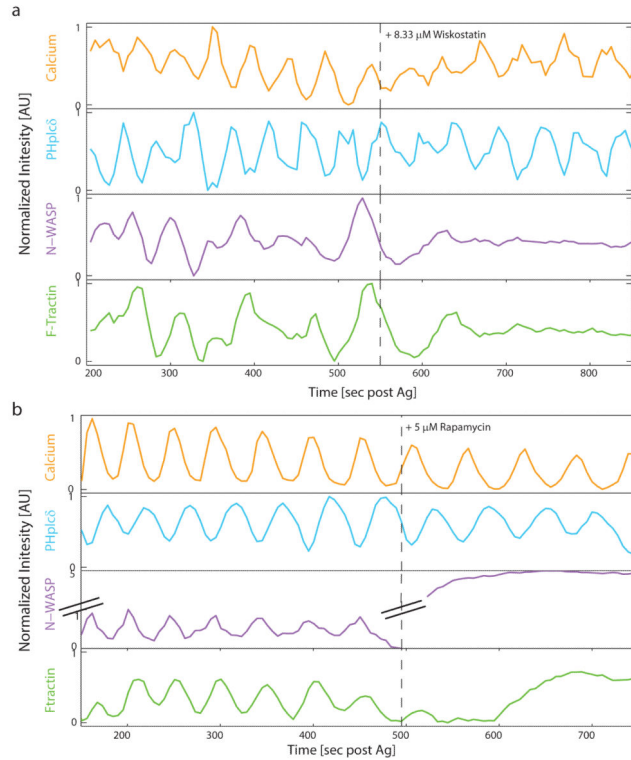
Figure 5. Inhibition of N-WASP dynamic inhibits F-actin oscillation without effecting Ca2+ and PI(4,5)P2 oscillations

a Wiskostatin-mediated inhibition of N-WASP and actin dynamics. Co-oscillation of pathway components after stimulation with antigen. The dashed line indicated addition of 8.33 μM N-WASP inhibitor Wiskostatin. **b** Inhibition of N-WASP dynamics via chemically induced FRB/FKBP dimerization of an inhibitory N-WASP construct. Co-oscillation of pathway components after stimulation with antigen. In this experiment, N-WASP was tagged with an FKBP and a non-flourescent plasma membrane targeted FRB domain was co-expressed. The dashed line indicated addition of 5 μM Rapamycin that induces dimerization of the FKBP and FRB domains which caused anchoring of N-WASP to the plasma membrane that resulted in inhibition of actin oscillations without any significant change in PI(4,5)P2 oscillations. Raw data for panels a & b is presented in Supp Table 1.
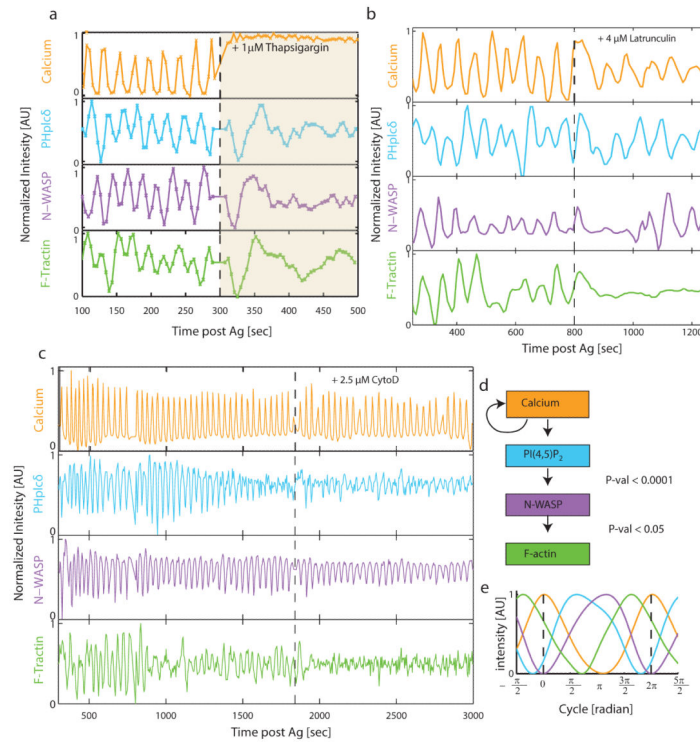
Figure 6. Synchronized phase-shifted oscillations of Calcium, PI(4,5)P2, N-WASP, and F-actin
Ca2+ oscillations drive cortical F-actin oscillations. **a** Example of a live-cell 5-channel analysis of Ca2+ (Fura2), PI(4,5)P2, N-WASP and F-actin signals shows synchronized oscillations. Stopping Ca2+ oscillations using the SERCA ER pump inhibitor thapsigargin blocks all oscillations. **b** Changes in the intensity of the four biosensor in a representative cell. The time is indicated when actin oscillations where inhibited using 4 μM Latrunculin. **c** Suppressing actin polymerization using cytocholasin D blocked F-actin oscillations but not the other oscillations. Raw data for panels a, b & c is presented in Supp Table 1. **d** Schematics of the Ca2+ pathway that generates coordinated cortical F-actin oscillations. P-value indicates probability that the lag between sequential biosensors is bigger than zero based on cross-correlation analysis of 83 cycles in 4 cells. **e** Average normalized cycle intensities of all cycles. Color codes are the same as in panels a and b.
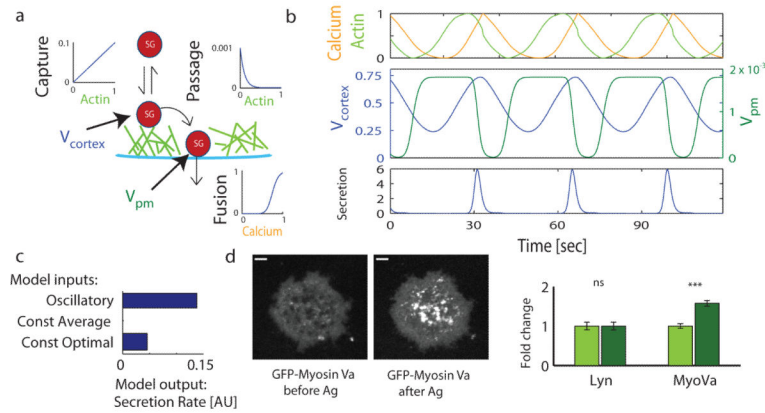
Figure 7. Mathematical model of how phase-shifted oscillations in cortical F-actin and Calcium correlates with a repetitive cycle of vesicle capture, passage and fusion to enhance secretion rates
a. Scheme of the mathematical model. (Inset) The F-actin and Ca2+ dependencies of the three vesicle state transitions, Capture, Passage and Fusion. Vcortex and V_{pm} are the respective concentrations of vesicles bound to actin cortex and plasma membrane. **b.** Simulation output of the model. The upper panel shows the model input: Ca2+ and F-actin oscillations. The middle panel shows the changes in the concentration of actin bound (blue) and plasma membrane bound (green) vesicles. The lower panel shows the output, the secretion rate. **c.** Comparison of model predictions of secretion rates for oscillatory and constant of F-actin and Ca2+ input levels. Two levels of constant Ca2+ and F-actin are shown: average, where the F-actin and Ca2+ levels are the mean of the oscillatory inputs and optimal where the levels where chose to maximize total secretion. **d**. Monitoring antigen-triggered recruitment of myosin Va, a motor protein that binds vesicles to F-actin and transports them. Left image panels show that recruitment of myosin Va occurs in the center where fusion occurs (maximum projection before and 2 minutes after antigen addition; scale-bar 5 μm). Right bar graph shows that, during F-actin oscillation cycles, the recruitment preferentially occurs when F-actin levels are high. As a control average intensity of a GFP membrane marker (Lyn) is compared to GFP-Myosin Va (MyoVa) during low actin (light green) and high actin (dark green) phases during oscillations. Errorbars are s.e.m, n = 83, p-value < 0.001 student t-test.
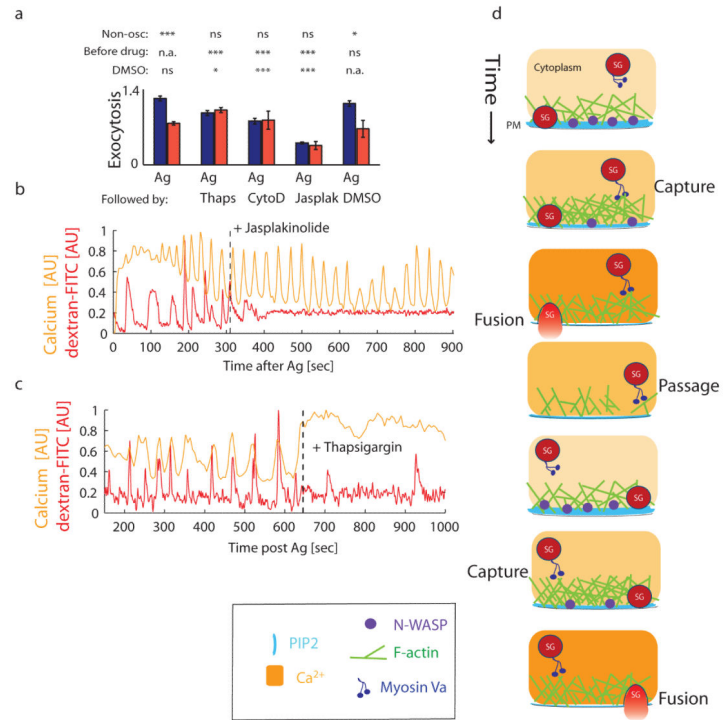
Figure 8. Direct measurements of enhancement in secretion due to Ca2+ and F-actin oscillations
a Bar diagram showing that secretion rates are more efficient for cells that oscillate (blue) compared to cells with elevated but non-oscillating Ca2+ levels (red). Addition of thapsigargin or cyotocholasin D to oscillating cells abolish the enhanced secretion without significantly affecting secretion when added to non-oscillating cells. Addition of Jasplakinolide abolished the oscillating cell's advantage and caused an additional overall reduction in secretion. Addition of DMSO is included as a control. (N-oscillating = 2891, N-non-oscillating = 4642 cells; errorbars are s.e.m. Result of t-tests comparing the exocytosis level of oscillating cells to non-oscillating, secretion before the addition of drug or secretion after addition of DMSO are presented above the bar plot., n.s. not statistically significant, * P-value<0.05 and *** P-value<0.001). **b** Example of an oscillating cell treated with Thapsigargin, showing that secretion slows even though the average Ca2+ level is higher. **c** Example of an oscillating cell treated with Jasplakinolide, showing that stabilizing the actin cortex inhibits secretion. **d** Schematics of the proposed secretion cycle based on phase shifted F-actin and Ca2+ oscillation cycles. In each cycle, Capture occurs at high F-actin, followed by Passage at low F-actin, followed by Fusion when Ca2+ levels subsequently increase. Note that changes in the cartoon are not to scale and for illustration purpose only.